International Journal of Solids and Structures 49 (2012) 2059–2065

Contents lists available at SciVerse ScienceDirect

International Journal of Solids and Structures

journal homepage: www.elsevier.com/locate/ijsolstr

Nonlinear hardening and softening resonances in micromechanical cantilever-nanotube systems originated from nanoscale geometric nonlinearities

Hanna Cho [a,*], Bongwon Jeong [a], Min-Feng Yu [a], Alexander F. Vakakis [a], D. Michael McFarland [b], Lawrence A. Bergman [b]

[a] Department of Mechanical Science and Engineering, University of Illinois at Urbana-Champaign, 1206 West Green Street, Urbana, IL 61801, USA
[b] Department of Aerospace Engineering, University of Illinois at Urbana-Champaign, 104 South Wright Street, Urbana, IL 61801, USA

ARTICLE INFO

Article history:
Received 6 January 2012
Received in revised form 5 April 2012
Available online 19 April 2012

Keywords:
Micromechanical cantilever oscillation
Nanotube
Geometric nonlinearity
Hardening
Softening
Multiple scales analysis

ABSTRACT

Micro/nanomechanical resonators often exhibit nonlinear behaviors due to their small size and their ease to realize relatively large amplitude oscillation. In this work, we design a nonlinear micromechanical cantilever system with intentionally integrated geometric nonlinearity realized through a nanotube coupling. Multiple scales analysis was applied to study the nonlinear dynamics which was compared favorably with experimental results. The geometrically positioned nanotube introduced nonlinearity efficiently into the otherwise linear micromechanical cantilever oscillator, evident from the acquired responses showing the representative hysteresis loop of a nonlinear dynamic system. It was further shown that a small change in the geometry parameters of the system produced a complete transition of the nonlinear behavior from hardening to softening resonance.

1. Introduction

Aiming for a wide range of applications, particularly in sensing, signal processing, and fundamental research, micro- and nano-mechanical resonators have been extensively studied in the last decade (Ekinci and Roukes, 2005; Kim and Chun, 2007). While transition from linear to nonlinear resonance was found to occur readily at these size scales, the underlying nonlinear characteristics have been largely trivialized (Ekinci and Roukes, 2005) or considered detrimental (Ekinci et al., 2004; Ekinci and Roukes, 2005; Kozinsky et al., 2006; Kacem and Hentz, 2009; Kacem et al., 2010) to the design objectives during the early development stage. Over the past few years, however, nonlinear dynamics in resonating systems at micro/nanoscale has drawn great attention as researchers begin to learn to tailor system properties to achieve novel applications (Rhoads et al., 2005; Lifshitz and Cross, 2008; Stanton et al., 2010). For example, using a doubly-clamped carbon nanotube, a nonlinear nanoresonator with tunable and broad bandwidth was developed, and its nonlinear instability was applied for sensing external perturbations such as extremely small changes in mass and energy dissipation in ambient environments (Cho et al., 2010).

The most commonly encountered nonlinear behavior in micro/nano-beam resonators, especially with doubly-clamped ends, is hardening resonance originated from the involvement of tension induced during the oscillatory transverse motion of the beam (Husain et al., 2003; Cho et al., 2010). Often this geometrically nonlinear behavior is combined with external perturbations such as nonlinear potential fields (Touze et al., 2004; Kacem and Hentz, 2009; Kacem et al., 2010; Mestrom et al., 2010; Rhoads et al., 2010; Elshurafa et al., 2011) and thermal radiation (Sahai et al., 2007; Sahai, 2010) to induce and study complex nonlinear dynamics such as backbone transitions between hardening and softening resonances. However, to introduce intrinsic nonlinearity into a widely used cantilever type micro/nanoscale beam resonator where there is one free end to relax the internal tension, special design considerations are needed. In this study, nonlinear dynamics was realized in a micromechanical cantilever type system by incorporating a nanotube coupling to introduce geometric nonlinearity intentionally.

We first analytically study the micromechanical cantilever system integrated with geometric nonlinearity to determine its dynamic behavior, and then demonstrate through experiment the predicted nonlinear response. The intentional integration of strong nonlinearity into an otherwise linear cantilever resonator generates rich dynamics such as hardening or softening resonances, as well as nonlinear hysteresis loops leading to instability jumps. The general finding of this work is that strong intentional stiffness nonlinearity can be efficiently induced in the micro- and nanoscale systems by appropriate implementation of geometric or kinematic nonlinearities of a linearly elastic stiffness element. In addition, somewhat counter-intuitively, we demonstrate that the appropriate incorporation of even a nanoscale element (a boron

* Corresponding author. Tel.: +1 2172440293.
E-mail address: cho25@illinois.edu (H. Cho).

0020-7683/$ - see front matter © 2012 Elsevier Ltd. All rights reserved.
http://dx.doi.org/10.1016/j.ijsolstr.2012.04.016

nitride nanotube) is sufficient to induce strong nonlinearity in a linear microscale dynamic system many orders of magnitude larger in size. To our knowledge, this is one of the first works reporting on intentional strong nonlinearity induced in a microsystem by a nanoscale attachment.

2. Description and modeling

The scanning electron microscope (SEM) images of the representative nonlinear system investigated in this work are presented in Fig. 1. It consists of two micromechanical cantilevers bridged between two free ends by a multi-walled boron nitride nanotube (BNNT). Titled view at 52° in SEM in Fig. 1(b) reveals that the two cantilevers are nearly coplanar. The attached BNNT is ~2.6 μm in length and ~80 nm in diameter. The two microcantilevers are separately anchored to a solid base, so the only mechanical coupling is through the attached BNNT. The end segments of the BNNT are rigidly fixed onto the surfaces of the free ends of the microcantilevers through localized e-beam induced deposition of platinum. In the absence of the nanotube, there is no mechanism to introduce stiffness nonlinearity into these two cantilevers, and their dynamics is linear within the range of their operation. The two microcantilevers are designed with their first eigenfrequencies sufficiently apart so that when one of the microcantilevers oscillates near its fundamental resonant frequency, the other is stationary and acts as a nearly fixed anchor for the nanotube. The microcantilevers couples through the attached nanotube and the major (and only) source of nonlinearity in our system is thus the stiffness nonlinearities induced in the nanotube when stretched axially at every period of oscillation of the microcantilever. Note that the nanotube is elastically soft in the lateral direction but comparatively rigid in the axial direction. As shown in the zoomed-in image in Fig. 1b, the gap between the free ends of the cantilevers is designed to be narrow to accommodate a short nanotube attachment at the scale of several micrometers in order to maximize the induced geometric nonlinearity. Using a simple lumped parameter model, we describe in the following the forced resonance of this intentionally nonlinear system; i.e., when one of the microcantilevers oscillates with a dominant frequency equal to that of the applied harmonic excitation.

2.1. Equations of motion

Fig. 2 shows the schematic model of the system shown in Fig. 1. The microcantilever oscillating in its fundamental mode is modeled by the vertical linear harmonic oscillator with mass (m), vertical spring (k_1), and viscous damper (c_1), excited by a harmonic force ($F_o \cos \omega t$). The microcantilever in a non-resonant state is modeled as the rigid ground. The nanotube is modeled as a massless linear spring (k_2), which introduces geometric nonlinearity into the system as the mass m displaces in the vertical direction. To be more general, considering that in a fabricated device there might exist a non-coplanar offset between the free ends of microcantilevers for attaching nanotube, we ascribe an initial offset (tilt) angle ϕ in the model for the attachment of the nanotube. It will be shown later that this angle plays an important role in the geometric nonlinearity induced in our system: depending on its value the system can produce either hardening or softening responses. Referring to the notation of Fig. 2, the length of the nanotube spring due to the vertical displacement of the mass (m) is $L_2' = \sqrt{y^2 + L_2^2 - 2yL\sin\varphi}$. The vertical component of the tension T in the nanotube caused by the oscillation of the microcantilever is then $T\cos\theta = k_2(L_2' - L_2)(y - L_2\sin\varphi)/L_2'$. Performing the balance of vertical forces applied on the mass (m) provides the following equation of motion of the microcantilever system with the coupling nanotube:

$$m\ddot{y} + c_1\dot{y} + k_1 y + T\cos\theta = F_o\cos\omega t \tag{1}$$

where overdot denotes differentiation with respect to time (t). Expanding the expression for the tension in the nanotube in Taylor series for small vertical displacements yields:

$$T\cos\theta = \left(k_2\sin^2\varphi\right)y - \left(\frac{3k_2L_2\sin\varphi}{2}\right)\left(\frac{y}{L_2}\right)^2 + \left(\frac{k_2L_2}{2}\right)\left(\frac{y}{L_2}\right)^3 + \ldots, \quad \left|\frac{y}{L_2}\right| << 1 \tag{2}$$

Here, we assumed small motions and small offset, i.e., $\varphi \ll 1$. Substituting Eq. (2) into Eq. (1) yields

$$m\ddot{y} + c_1\dot{y} + \tilde{k}_1 y + \tilde{k}_2 y^2 + \tilde{k}_3 y^3 = F_o\cos\omega t \tag{3}$$

where

$$\tilde{k}_1 = k_1 + k_2\sin^2\varphi, \quad \tilde{k}_2 = -\frac{3k_2}{2L_2}\sin\varphi, \quad \tilde{k}_3 = \frac{k_2}{2L_2^2}. \tag{4}$$

As expected, the nanotube spring introduces the cubic nonlinearity into the system, regardless of the existence of the offset angle. However, the offset angle φ contributes to both the quadratic and linear spring constants of the system. This means that depending on the

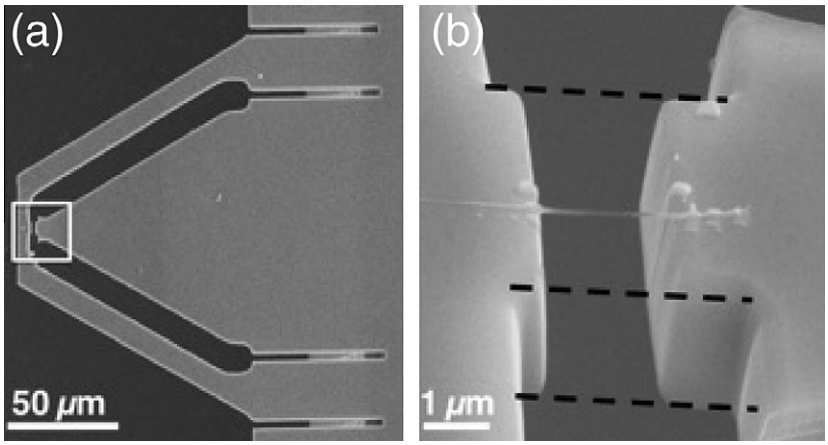

Fig. 1. SEM images of a nonlinear microcantilever system with integrated geometric nonlinearity through a nanotube attachment: (a) two micromechanical cantilevers are coupled through a nanotube, and (b) a magnified view of the marked region in square in (a) imaged at a sample tilt angle of 52°. The attached BNNT is ~2.6 μm in length and ~80 nm in diameter.

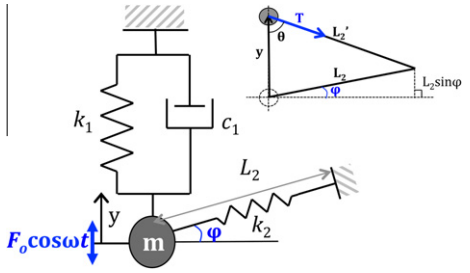

Fig. 2. Schematic representation of the microcantilever system integrated with a nanotube coupling. The inset shows the geometry parameter related to the stretch of the attached nanotube.

value of this angle either the hardening effect due to the cubic stiffness term or the softening effect due to the quadratic stiffness term can potentially dominate in the dynamic response of the system. Note that the system with $\varphi = 0$ is a typical Duffing oscillator with a hardening spring as the sign of k_3 is always positive.

To facilitate the analysis, Eq. (3) is normalized by introducing the nondimensional variables,

$$\bar{y} = \frac{y}{L_2}, \quad \tau = \tilde{\omega}_o t \tag{5}$$

where $\tilde{\omega}_o$ is the linearized resonant angular frequency,

$$\tilde{\omega}_o = \sqrt{\frac{\tilde{k}_1}{m}} \approx \sqrt{\frac{k_1}{m}} + \frac{k_2}{2m}\sin^2\varphi. \tag{6}$$

We note here that the resonant frequency of the system is augmented by the additional stiffness from the vertical component of the nanotube spring due to the offset angle. Finally, the equation of motion in nondimensionalized form is expressed as,

$$\bar{y}'' + 2\zeta\bar{y}' + \bar{y} + a_2\bar{y}^2 + a_3\bar{y}^3 = q_o\cos\Omega\tau \tag{7}$$

where prime denotes differentiation with respect to dimensionless time τ. The parameters appearing in Eq. (7) are given by:

$$2\zeta = \frac{c_1}{m\tilde{\omega}_o}, \quad q_o = \frac{F_o}{\tilde{k}_1 L_2}, \quad \Omega = \frac{\omega}{\tilde{\omega}_o},$$

$$a_2 = \frac{\tilde{k}_2}{\tilde{k}_1}L_2 = -\frac{3}{2}\frac{k_2\sin\varphi}{k_1 + k_2\sin^2\varphi}, \quad a_3 = \frac{\tilde{k}_3}{\tilde{k}_1}L_2^2 = \frac{k_2}{2(k_1 + k_2\sin^2\varphi)}. \tag{8}$$

2.2. Multiple scales analysis

The method of multiple scales (Nayfeh and Mook, 1995) is employed to find the dynamic response of the system at the fundamental mode resonance of the microcantilever; i.e., $\Omega \approx 1$. To obtain a uniformly valid approximate solution, we need to order each term so that damping, excitation, and nonlinear terms appear at the same time scale in the perturbation scheme. We introduce the small parameter ε and the rescalings $y \to \varepsilon y$, $2\zeta \to 2\varepsilon^2\zeta$, and $q_0 \to \varepsilon^3 q_0$. The small parameter ε represents the (small) amplitude of the oscillation of the microcantilever. Accordingly, Eq. (7) is scaled as

$$y'' + 2\varepsilon^2\zeta y' + y + \varepsilon a_2 y^2 + \varepsilon^2 a_3 y^3 = \varepsilon^2 q_o\cos\Omega\tau \tag{9}$$

The proximity of the excitation frequency to the linearized resonant frequency is represented by introducing the detuning parameter σ, giving

$$\Omega = 1 + \varepsilon^2\sigma. \tag{10}$$

Then, we define multiple time scales explicitly as $T_n = \varepsilon^n\tau$, and the periodic solution is sought in the form of

$$y(\tau;\varepsilon) = y_o(T_o, T_1, T_2) + \varepsilon y_1(T_o, T_1, T_2) + \varepsilon^2 y_2(T_o, T_1, T_2). \tag{11}$$

Because the analysis is carried out to order ε^2, the slow time scales are introduced up to the same order. The derivative with respect to nondimensionalized time is expressed using scaled independent time scales as

$$\frac{\mathrm{d}}{\mathrm{d}\tau} = \frac{\partial}{\partial T_o} + \varepsilon\frac{\partial}{\partial T_1} + \varepsilon^2\frac{\partial}{\partial T_2} \equiv D_o + \varepsilon D_1 + \varepsilon^2 D_2 \tag{12}$$

Substituting Eq. (11) and Eq. (12) into Eq. (9) and matching coefficients of equal powers of ε, one obtains a series of sub-problems:

$$O(\varepsilon^0) : D_o^2 y_o + y_o = 0 \tag{13}$$

$$O(\varepsilon^1) : D_o^2 y_1 + y_1 = -2D_oD_1y_o - a_2y_o^2 \tag{14}$$

$$O(\varepsilon^2) : D_o^2 y_2 + y_2 = -2D_oD_1y_1 - 2D_oD_2y_o - D_1^2y_o^2 - 2\zeta D_o y_o - 2a_2y_oy_1 - a_3y_o^3 + q_o\cos(T_o + \sigma T_2) \tag{15}$$

The solution of Eq. (13) is

$$y_o = A(T_1, T_2)e^{jT_o} + cc \tag{16}$$

where A is a complex describing the slowly varying modulus of the amplitude, cc denotes the complex conjugate, and $j = (-1)^{1/2}$. Substituting Eq. (16) into Eq. (14), removing secular terms, and setting $A = A(T_2)$, the solution of Eq. (14) is expressed as:

$$y_1 = a_2\left[-A\bar{A} + \frac{1}{3}A^2e^{2jT_o}\right] + cc. \tag{17}$$

Substituting Eq. (16) and Eq. (17) into Eq. (15) and again eliminating secular terms give the modulation equation describing the temporal evolution of the slowly varying modulus:

$$2jA' + 2j\zeta A + \left(3a_3 - \frac{10}{3}a_2^2\right)A^2\bar{A} + \frac{1}{2}q_oe^{j\sigma T_2} = 0 \tag{18}$$

The slowly varying complex amplitude is then expressed in polar form as $A = (1/2)\alpha e^{j\beta}$, where the amplitude α and the phase β are real valued functions of the slow time scale T_2. Separating the real and imaginary parts and introducing the phase difference $\gamma \equiv \sigma T_2 - \beta$ to eliminate terms depending on time explicitly, we derive a set of autonomous modulation equations that governs the slow flow dynamics of the system:

$$\begin{aligned} \alpha' &= -\zeta\alpha - \frac{q_o}{2}\sin\gamma \\ -\alpha\gamma' &= \sigma\alpha - \left(\frac{3}{8}a_3 - \frac{10}{24}a_2^2\right)\alpha^3 - \frac{q_o}{2}\cos\gamma \end{aligned} \tag{19}$$

Hence, the approximate solution to the system with accuracy $O(\varepsilon^2)$ is obtained as,

$$y(\tau) = \alpha\cos(\Omega\tau + \gamma) - \varepsilon\frac{1}{2}a_2\alpha^2 + \varepsilon\frac{1}{6}a_2\alpha^2\cos(2\Omega\tau + 2\gamma) + O(\varepsilon^2), \tag{20}$$

where α and γ are defined by Eq. (19). We obtain the steady-state solutions of Eq. (19) by setting $\alpha' = \gamma = 0$, which gives the relation between steady-state amplitude and frequency as,

$$\left[\zeta^2 + \left(\sigma - \frac{9a_3 - 10a_2^2}{24}\alpha_{ss}^2\right)^2\right]\alpha_{ss}^2 = \pm\frac{q_o^2}{4}, \quad \gamma = \pm\frac{\pi}{2}, \tag{21}$$

where subscript ss denotes steady-state.

2.3. Nonlinear hardening and softening resonances

The approximate periodic solution of Eq. (20) indicates that the motion of the mass is not centered at $y = 0$ but shifted by $-(\varepsilon/2)a_2\alpha^2$. This is due to the quadratic nonlinearity originated

from the tension component in y from the attached nanotube with an offset angle of φ. When this angle is positive (negative), the vertical spring is initially under compression (tension), which results in an upward (downward) shift of the motion.

Examining the frequency response of the system in steady-state for the fundamental resonance described in Eq. (21), the effect of offset angle becomes more consequential. We derive the backbone curves for the corresponding Hamiltonian system, i.e., the undamped and unforced oscillator, resulted from Eq. (21) by setting $\zeta = q_o = 0$. This produces the following approximate frequency-steady state amplitude curve:

$$\alpha_{ss} = \pm\left(\frac{24}{9a_3 - 10a_2^2}\sigma\right)^{1/2}. \tag{22}$$

As shown from this equation, the sign of the coefficient of the frequency detuning parameter determines whether the dynamics of the system exhibits nonlinear softening or hardening resonance. Accordingly, we define a parameter $\mu = 9a_3 - 10a_2^2$ quantifying the degree of nonlinearity in the system. Substituting the physical parameters into the expression for μ gives the critical offset angle φ_{cr} required to eliminate both hardening and softening nonlinear behavior by counterbalancing the effect of the quadratic and cubic terms:

$$\sin^2\varphi_{cr} = \frac{k_1}{4k_2}. \tag{23}$$

When the offset angle is smaller than this critical angle, the nonlinear dynamic response is a hardening one, and otherwise, the response a softening one.

3. Device fabrication and experimental setup

The nonlinear cantilever system was fabricated with micromachining and nanomanipulation. First, the two micromechanical cantilevers were fabricated with a Silicon-on-Insulator (SOI) wafer having a 2 μm thick device layer (Si), 2 μm thick buried insulator layer (SiO_2), and 400 μm thick substrate layer (Si). The device layer forms a cantilever structure, whereas the substrate layer serves as a base of the suspended cantilevers. The general steps of the fabrication involved the positive photoresist (SPR-220) coating of both the top and bottom surfaces of the SOI wafer; the patterning of the photoresist with photolithography according to the design of the cantilevers and the anchoring base; the etching of the top Si layer to define the cantilevers; and the Deep Reactive Ion Etching (DRIE) of the wafer backside to define the anchoring base. In the last step, the wafer was immersed in hydrofluoride (HF) solution to etch away the buried oxide layer to release the cantilevers from the wafer to realize the freestanding formation of the cantilevers.

The micromachining process provides two micromechanical cantilevers connected to each other at the free ends. Focused ion beam cutting was applied to cut through a narrow gap between the ends of the two cantilevers to separate them. A high quality BNNT was then selected and manipulated inside a SEM with a nanomanipulator and placed across the narrow gap. Finally, both ends of the placed BNNT were fixed on the cantilever surface by electron beam-induced deposition of a small amount of platinum.

The cantilever system was driven by a piezoelectric stack placed underneath the cantilever-anchoring base in an air ambient environment. A sinusoidal AC driving signal supplied from a function generator actuated the stack. The frequency was first swept up and then down, and the oscillation amplitude at the end of the cantilever was measured using a laser Doppler Microvibrometer (Polytec UHF-120). Fast Fourier transform (FFT) of the data collected from the vibrometer at each driving frequency provided the spectral response of the system. It is noted that nonlinearity is not introduced in either the actuation with the piezoelectric stack, or the measurement laser of the vibrometer operated at a constant power less than 5 mW.

4. Experimental results

4.1. Linear resonances of dual cantilevers without a nanotube attachment

In order to test the assumptions in our model, the responses of the inner and outer microcantilevers before coupled through nanotube were measured. The experimental results are plotted in Fig. 3 and are fitted with solid curves according to the model of a forced linear harmonic oscillator. The responses of both cantilevers closely follow the fitting curves; hence, in the absence of the nanotube, the dynamics of these microcantilevers is reasonably within the linear regime over their operational ranges. The fundamental frequencies, damping coefficients, and base excitation amplitudes of the piezoelectric stack are estimated to be 196.8 kHz, 0.0022, and 1.24 nm for the inner cantilever and 121.1 kHz, 0.0033, and 1.28 nm for the outer cantilever, respectively. It is important to note that the fundamental eigenfrequencies of the inner and outer microcantilevers are located enough apart, so there is no significant coupling between them.

4.2. Nonlinear hardening resonance

Fig. 4 shows the experimentally acquired hardening resonances for the inner cantilever in the system configuration shown in Fig. 1. The results from Fig. 4a to f correspond to a monotonic increase of the oscillation amplitude with the increase of the driving amplitude. The circles/crosses in the plots denote the acquired steady-state experimental measurements made during the upward/downward frequency sweeps, respectively. The measurement was performed on a device having an almost perfect coplanar alignment between the cantilevers as shown in Fig. 1b (i.e., the offset angle $\varphi = 0$). Thus, the quadratic term in the equation of motion is negligible, which leads to hardening resonances. At small amplitude oscillation, as shown in Fig. 4a, the dynamic response remains nearly linear because the axial tension induced in the nanotube is insignificant. As the oscillating amplitude increases, however, the spectral curves begin to bend toward higher frequencies as a result of the hardening effect introduced from an axially stretched nanotube, and leading to hysteresis loops including the well-documented discontinuous jumps. The displacement of the outer beam within the frequency range of interest was also

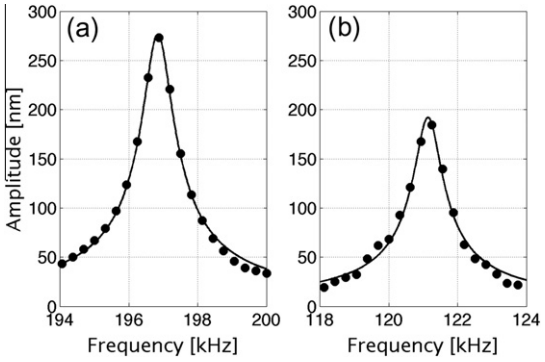

Fig. 3. Experimentally acquired linear responses (solid circle) for the inner (a) and outer (b) microcantilevers shown in Fig 1, measured from the microcantilevers with no nanotube coupling. The solid lines are the fitting curves based on the model of a forced linear harmonic oscillator.

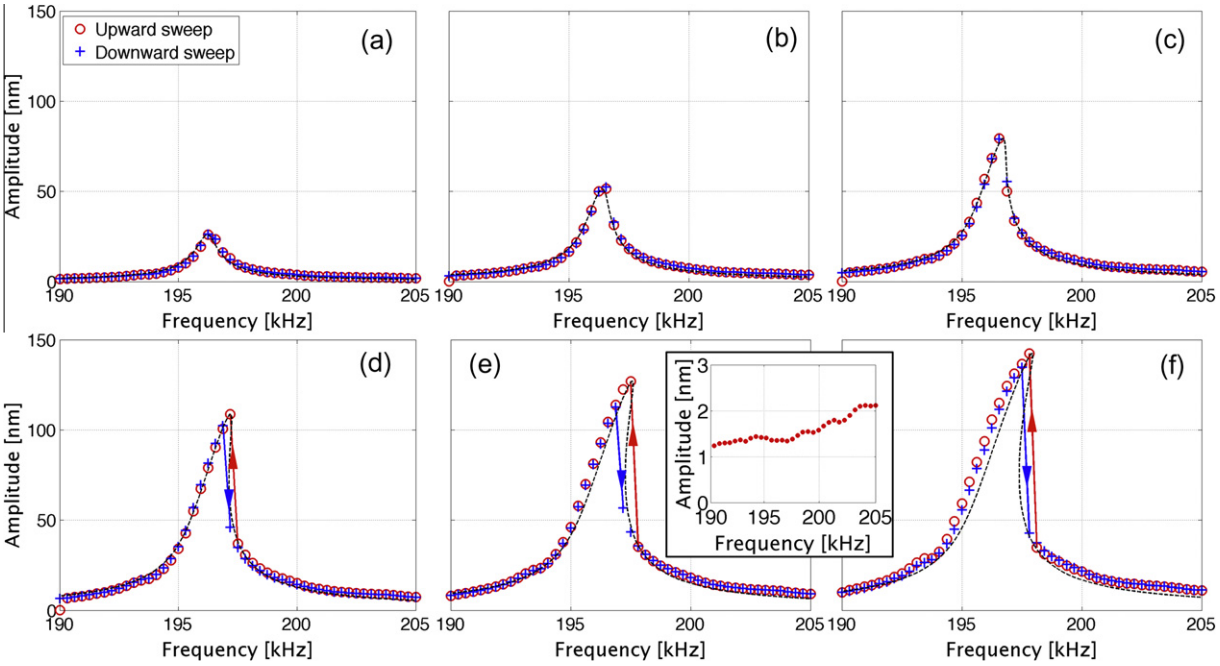

Fig. 4. Experimentally acquired hardening resonances for the inner microcantilever shown in Fig. 1 with increasing driving amplitude. The dashed lines are the fitting curves based on the developed model described in the text. The inset in (e) represents the response of the outer cantilever within the frequency range of interest, of which amplitude is in the same order of magnitude as the base excitation amplitude.

examined, as shown in the inset of Fig. 4e, to be comparable to the base excitation amplitude, confirming its non-resonance state.

The experimental results were compared with the analytical model results presented in the previous sections. The linearized fundamental resonant frequency (f_o) and the nonlinear constant (μ) were estimated by fitting the maximum amplitude values of the response curves into the backbone curve described by Eq. (22). The fitting, as shown in Fig. 5, gives $f_o = 196.7$ kHz and $\mu = 1.06 \times 10^{-5}$. The damping coefficient (ζ) of the cantilever was obtained from curve fitting to the response curves acquired at small oscillation amplitude and was found to be ~0.0023. Finally, the equivalent applied forces (q_0) were obtained by fitting the drop-jump instabilities in the backbone curve. Substituting those estimated parameters into Eq. (21), the corresponding frequency responses predicted by the model were plotted with dashed lines in Fig. 4, which showed good agreement with the experimental results. The discrepancy between model and experiment grows as the driving force increases, possibly due to the amplitude-dependent increase in damping of the cantilever itself. The increased energy dissipation through the deformation of the nanotube (Jiang et al., 2004; Yum et al., 2004), which is not considered in our analysis, may also be partly responsible for the increased discrepancy.

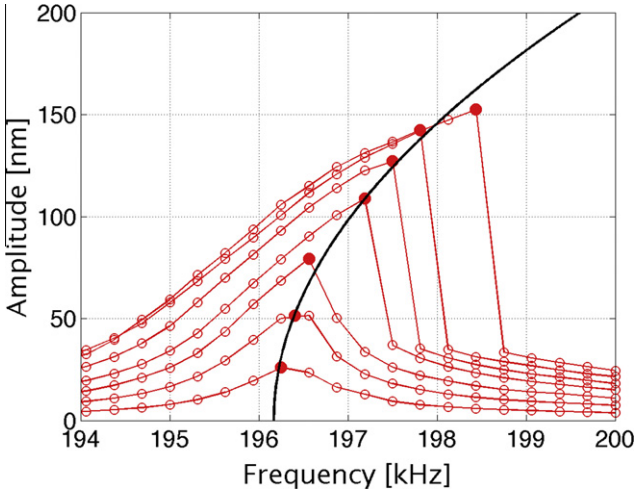

Fig. 5. Backbone curve fit for the hardening resonances presented in Fig. 4. The maximum oscillation amplitude in each resonance response (red circle) under given driving amplitude is fitted into a modeled backbone curve (in black) for the nonlinear system. (For interpretation of the references to colour in this figure legend, the reader is referred to the web version of this article.)

4.3. Nonlinear softening resonance

In the microcantilever system having non-coplanar cantilever surfaces as shown in Fig. 6b, the attached nanotube is severely tilted off the reference ground plane. Such a microcantilever system showed a clear softening response as shown in Fig. 7. As explained previously, such a softening response is a direct result of the tilting in the nanotube coupling attachment and the consequent introduction of a strong quadratic term in Eq. (23). Following the procedures explained in Section 4.1, the relevant parameters were estimated enabling comparison of experimental results with those predicted by the model. The backbone curve in Fig. 8, derived singly from data acquired at low oscillation amplitude, failed to predict the experimentally acquired response at high oscillation amplitude. Thus, two sets of parameters (f_o, μ), (105.4 kHz, -3.6×10^{-5}) and (103.1 kHz, -2.6×10^{-6}) for low and high amplitude oscillations, respectively, are used to fit the experimental data over the entire frequency range. Such different responses at different oscillation amplitudes were believed to be originated from the different spring type of behaviors of the attached nanotube underwent different magnitudes of deformation. When there is an initial offset angle, the axial stress applied to the attached nanotube during dynamic oscillation of the cantilever is divided into two regimes; i.e., one compression-dominated at low oscillating amplitude and another tension-dominated at high oscillating amplitude. Note that the nanotube experiences only tensile strain

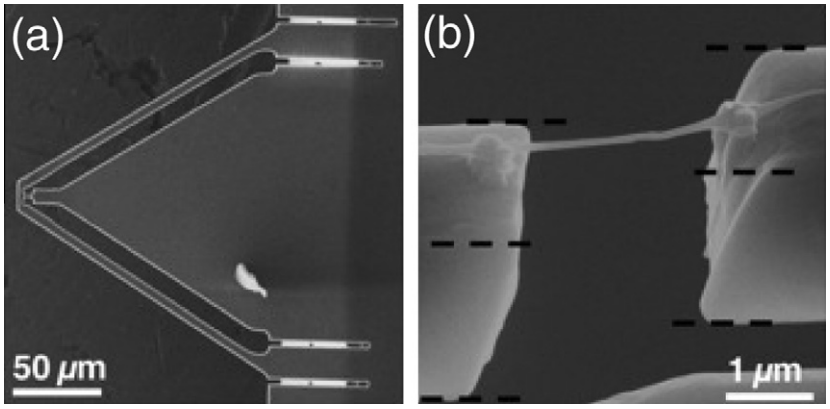

Fig. 6. SEM images of a nonlinear microcantilever system exhibiting softening responses due to the non-coplanar attachment of the nanotube. (a) The overall view of the microcantilever system consisting of two separate microcantilevers. (b) The amplified view around the gap between the free ends of two microcantilevers showing the nanotube attachment. The SEM image is acquired at a sample tilt of 52° showing the non-coplanar offset of the free ends of the microcantilevers. The attached BNNT is ~2.4 μm in length and ~75 nm in diameter.

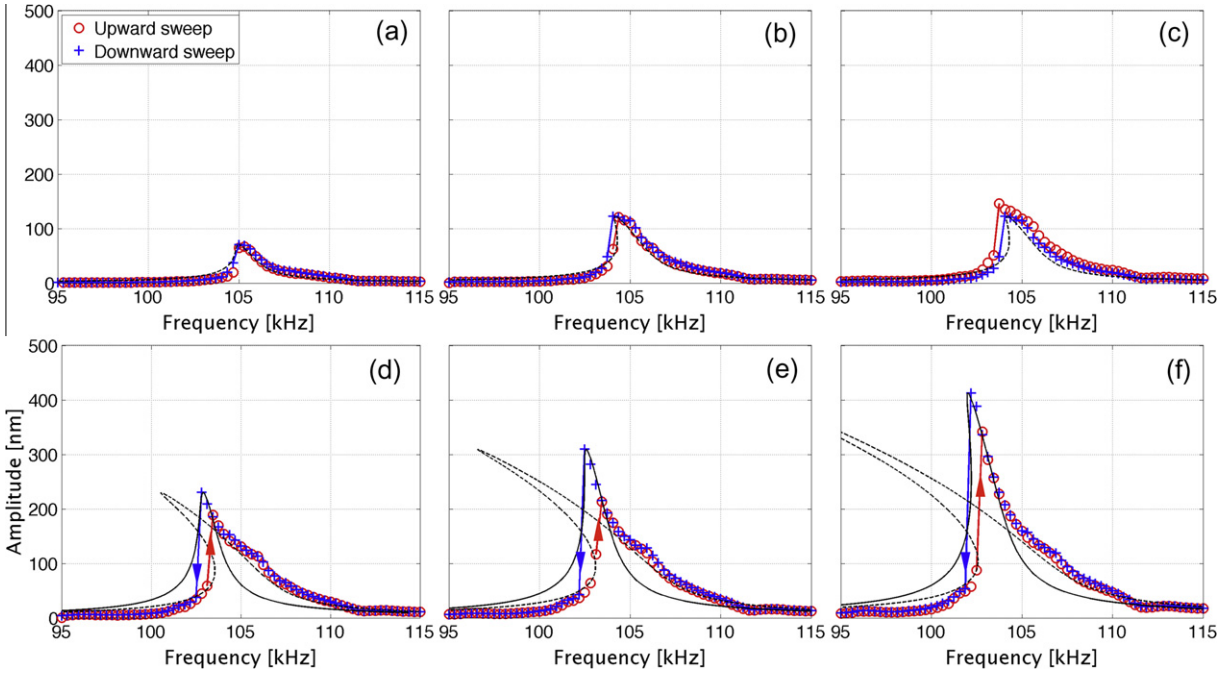

Fig. 7. Experimentally acquired softening responses of the inner microcantilever shown in Fig. 6. Two fitting curves are plotted based on the parameters estimated from backbone curve fitting shown in Fig. 8. The dashed/solid curves represent the nonlinear responses of the system in the compression/tension-dominated regimes of the attached nanotube, respectively.

due to axial stretch by oscillatory motion of the cantilever in the absence of this offset angle. Due to its high aspect ratio structure, a nanotube under compression can exhibit elastic Euler buckling (or rippling bending) at small compressive strain, resulting in a reduction in its stiffness (Yap et al., 2007). Alternately, a nanotube in tension can sustain high tensile strain, maintaining high axial stiffness until failure (Yu et al., 2000). The difference in axial stiffness in tension and compression contributes to the difference in the nonlinear constant (μ) between the tension- and compression-dominated regimes. Besides, in the tension-dominated regime, the effect of offset angle is negligible compared with the nonlinear effect induced by axial stretch of the nanotube, which leads to the reduction in the estimated fundamental resonant frequency (f_o) from 105.4 kHz to 103.1 kHz according to Eq. (6).

Two sets of responses are thus determined from the model and plotted in Fig. 7; dashed and solid lines used fitting parameters obtained in compression-dominated and tension-dominated regions, respectively. When the amplitude of oscillation is small, the experimentally measured response follows the dashed line. Thereafter, as the oscillation amplitude increases, the slope of the upper stable branch increases to follow the solid line. It is interesting to note that the small shoulder experimentally observed in the upper branch near the intersection of the two fitted curves is indicative of the transition from the compression-dominated to the tension-dominated regime as discussed.

5. Summary and conclusions

In micro/nanomechanical resonating systems, the onset of nonlinear dynamics is more readily realizable than in macroscale devices due to their small size and typically low mechanical

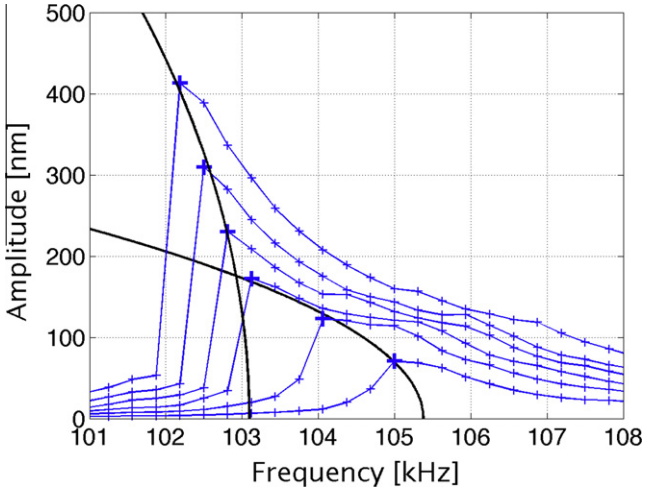

Fig. 8. Backbone curve fitting for the softening resonances presented in Fig. 7. To describe the entire range of dynamic response, two backbone curves (in black) from two different sets of fitting parameters for f_o and μ are used to fit the responses (blue cross), reflecting the different mechanical behaviors of the attached nanotube under compression at small oscillation amplitude and tension at large oscillation amplitude. (For interpretation of the references to colour in this figure legend, the reader is referred to the web version of this article.)

damping. This allows the system to be operated in relative large amplitude that can introduce noticeable amount of geometric and kinematic nonlinearities. In this study, we provided a novel design of a nonlinear resonator over a typical microcantilever by integrating geometric nonlinearity through a nanotube attachment. While the nanotube attachment hardly affected the overall mass of the system, it introduced, very effectively, strong geometric nonlinearities that totally transformed an otherwise purely linear system into a strong nonlinear dynamic system. Furthermore, we showed, through theoretical modeling, that a simple introduction of offset in the attachment of the nanotube could readily tune the system into a nonlinear system with either a hardening response or a softening response exploiting the different mechanical deformation behaviors of the attached nanotube under tension or compression. The model analysis was quantitatively and qualitatively corroborated with experiment results.

We expect that such microcantilever systems incorporating intentional nonlinearity can be exploited for sensing applications similar to that demonstrated in a relevant nonlinear nanoresonator (Cho et al., 2010), especially in a practical environment (i.e., room temperature and/or atmospheric pressure) owing to its readily achievable relatively large oscillation amplitude. Introducing such a design into dynamic atomic force microscopy (AFM) imaging can also be potentially beneficial in terms of increasing the bandwidth and stability of the dynamic AFM operation (Cho et al., in press). The designed introduction of intentional nonlinearity into microscale and nanoscale dynamic mechanical systems combined with the inherent ease of realization of nonlinearity at micro/nanoscale can surely significantly enrich the complexity of dynamics in such systems, and consequently allow the design of more advanced control and sensing schemes in such micro/nanoscale system to achieve specific performance objectives. Of course, this calls for further extensive study of the underlying nonlinear behavior of such systems, especially incorporating fuller understanding of the mechanical behavior of the critical element in the systems, namely the nanotube or nanowire.

Acknowledgement

The authors acknowledge the financial support of the National Science Foundation (NSF) under Grant Nos. CMMI-0726878 and CMMI-100615.

References

Cho, H., Yu, M.-F., Vakakis, A.F., Bergman, L.A., McFarland, D.M., 2010. Tunable, broadband nonlinear nanomechanical resonator. Nano. Lett. 10, 1793–1798.
Cho, H., Yu, M.-F., Vakakis, A.F., Bergman, L.A., McFarland, D.M., in press. Integration of geometric nonlinearity for stable and broadband nonlinear atomic force microscopy. Surf. Sci.
Ekinci, K.L., Roukes, M.L., 2005. Nanoelectromechanical systems. Rev. Sci. Instrum. 76, 061101.
Ekinci, K.L., Yang, Y.T., Roukes, M.L., 2004. Ultimate limits to inertial mass sensing based upon nanoelectromechanical systems. J. Appl. Phys. 95, 2682–2689.
Elshurafa, A.M., Khirallah, K., Tawfik, H.H., Emira, A., Abdel Aziz, A.K.S., Sedky, S.M., 2011. Nonlinear dynamics of spring softening and hardening in folded-MEMS comb drive resonators. J. Microelectromech. Syst. 20, 943–958.
Husain, A., Hone, J., Postma, H., Huang, X., Drake, T., Barbic, M., Scherer, A., Roukes, M.L., 2003. Nanowire-based very-high-frequency electromechanical resonator. Appl. Phys. Lett. 83, 1240–1242.
Jiang, H., Yu, M.-F., Liu, B., Huang, Y., 2004. Intrinsic energy loss mechanisms in a cantilevered carbon nanotube beam oscillator. Phys. Rev. Lett. 93, 185501.
Kacem, N., Hentz, S., 2009. Bifurcation topology tuning of a mixed behavior in nonlinear micromechanical resonators. Appl. Phys. Lett. 95, 183104.
Kacem, N., Arcamone, J., Perez-Murano, F., Hentz, S., 2010. Dynamic range enhancement of nonlinear nanomechanical resonant cantilevers for highly sensitive NEMS gas/mass sensor applications. J. Micromech. Microeng. 20, 045023.
Kim, H.C., Chun, K., 2007. RF MEMS technology. IEE J. Trans. 2, 249–261.
Kozinsky, I., Postma, H.W.C., Bargatin, I., Roukes, M.L., 2006. Tuning nonlinearity, dynamic range, and frequency of nanomechanical resonators. Appl. Phys. Lett. 88, 253101.
Lifshitz, R., Cross, M.C., 2008. Nonlinear dynamics of nanomechanical and micromechanical resonators, Reviews of Nonlinear Dynamics and Complexity. Wiley-VCH Verlag GmbH & Co. KGaA, Weinheim, Germany.
Mestrom, R.M.C., Fey, R.H.B., Phan, K.L., Nijmeijer, H., 2010. Simulations and experiments of hardening and softening resonances in a clamped–clamped beam MEMS resonator. Sens. Actuat. A – Phys. 162, 225–234.
Nayfeh, A.H., Mook, D.T., 1995. Nonlinear Oscillations. Wiley.
Rhoads, J., Shaw, S., Turner, K., Baskaran, R., 2005. Tunable microelectromechanical filters that exploit parametric resonance. J. Vib. Acoust. 127, 423–430.
Rhoads, J.F., Shaw, S.W., Turner, K.L., 2010. Nonlinear dynamics and its applications in micro- and nanoresonators. J. Dyn. Sys., Meas. Contr. 132, 034001.
Sahai, T., 2010. Backbone transitions and invariant tori in forced micromechanical oscillators with optical detection. Nonlinear Dyn. 62, 273–289.
Sahai, T., Bhiladvala, R., Zehnder, A.T., 2007. Thermomechanical transitions in doubly-clamped micro-oscillators. Int. J. Non-Linear Mech. 42, 596–607.
Stanton, S., McGehee, C., Clark, C.M., Mann, B.P., 2010. Nonlinear dynamics for broadband energy harvesting: Investigation of a bistable piezoelectric inertial generator. Physica D 239, 640–653.
Touze, C., Thomas, O., Chaigne, A., 2004. Hardening/softening behaviour in nonlinear oscillations of structural systems using non-linear normal modes. J. Sound Vib. 273, 77–101.
Yap, H.W., Lakes, R.S., Carpick, R.W., 2007. Mechanical instabilities of individual multiwalled carbon nanotubes under cyclic axial compression. Nano. Lett. 7, 1149–1154.
Yu, M.-F., Louie, O., Dyer, M.J., Moloni, K., Kelly, T.F., Ruoff, R.S., 2000. Strength and breaking mechanism of multiwalled carbon nanotubes under tensile load. Science 287, 637–640.
Yum, K., Wang, Z., Suryavanshi, A.P., Yu, M.-F., 2004. Experimental measurement and model analysis of damping effect in nanoscale mechanical beam resonators in air. J. Appl. Phys. 96, 3933–3938.